Organic Memory Device Fabricated Through Solution Processing

JIANYONG OUYANG, CHIH-WEI CHU, RICKY JIA-HUNG TSENG, ANKITA PRAKASH, AND YANG YANG

Contributed Paper

Novel organic memory devices including nonvolatile and write-once-read-many-times memory devices are reported. These devices were fabricated through a simple solution processing technique. Programmable electrical bistability was observed on a device made from a polymer film containing metal nanoparticles capped with saturated alkanethiol and small conjugated organic compounds sandwiched between two metal electrodes. The pristine device, which was in a low-conductivity state, exhibited an abrupt increase of current when the device was scanned up to a few volts. The high-conductivity state can be returned to the low-conductivity state by applying a certain voltage in the reverse direction. The device has a good stability in both states, and the transition from the low- to the high-conductivity state takes place in nanoseconds, so that the device can be used as a low-cost, high-density, high-speed, and nonvolatile memory. The electronic transition is attributed to the electric-field-induced charge transfer between the metal nanoparticles and small conjugated organic molecule. The electrical behavior of the device is strongly dependent on the materials in the polymer film. When gold nanoparticles capped with aromatic thiol were used, the device exhibited a transition from low- to high-conductivity state at the first voltage scan, and the device in the high-conductivity state cannot be returned to the low-conductivity state. This device can be used as a write-once-read-many-times memory device.

Keywords*—Charge transfer, electrical bistable, memory, metal nanoparticles, organic, polymer.*

I. Introduction

Organic semiconducting materials exhibit strong potential to be the active materials in almost all kinds of electronic devices. During the past ten years, organic LEDs [1], [2], organic photovoltaic cells [3], and organic transistors [4] made great progress, and some were even commercialized. Organic electronic devices demonstrate unique advantages compared with the inorganic semiconductor devices. These include low fabrication cost, high mechanical flexibility, and versatility of the material chemical structure. However, electronic memory using organic materials is still in the exploration stage. A high-performance organic memory will have a strong impact on rapidly developing information technology and will be an important player in flexible electronics. Though three-terminal transistors, using ferroelectric polymers [5], and two-terminal bistable devices, which exploit charge transfer between metal atoms and organic compounds [6], [7], exhibit interesting performance, they are far from practical applications in memories. A new electronic bistable device with a triple-layer structure, two organic layers, and a middle discontinuous metal layer, sandwiched between two metal electrodes, exhibits promising performance and can be used as a nonvolatile memory [8]–[10]. However, the fabrication of this device is through thermal evaporation in high vacuum, and stringent conditions are required to control the morphology of the middle, discontinuous metal layer. Recently, Möller *et al.* reported a memory device using conducting polymers, but this device can be written only once and cannot be used as nonvolatile memory [11]. A two-terminal electronic bistable device, which can be fabricated through solution processing and can be written/erased many times, should be the target for organic memory.

In this paper, we describe the fabrication and operation of two kinds of organic memory devices: nonvolatile memory devices [12] and write-once-read-many-times memory devices [13]. The active layer of these devices was fabricated by solution processing, and the device exhibited high performance. They are potentially competitive with inorganic memory in some ways and potentially outperform it in others. For example, they can be processed in three-dimensional arrays for very high density storage and have high flexibility to be compatible with other organic devices.

Manuscript received August 20, 2004; revised February 22, 2005. This work was supported by the Air Force Office of Scientific Research.

The authors are with the Department of Materials Science and Engineering, University of California, Los Angeles, CA 90095 USA (e-mail: ouyangj@ucla.edu; gchu@ucla.edu; jhtseng@ucla.edu; ankita@seas.ucla.edu; yangy@ucla.edu).

Digital Object Identifier 10.1109/JPROC.2005.851235

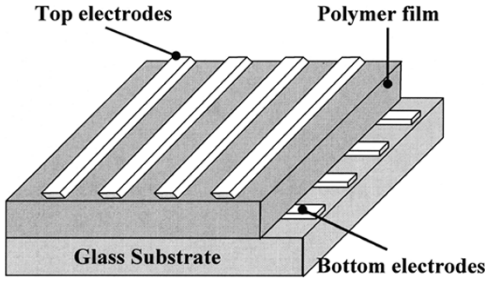

Fig. 1. Device structure.

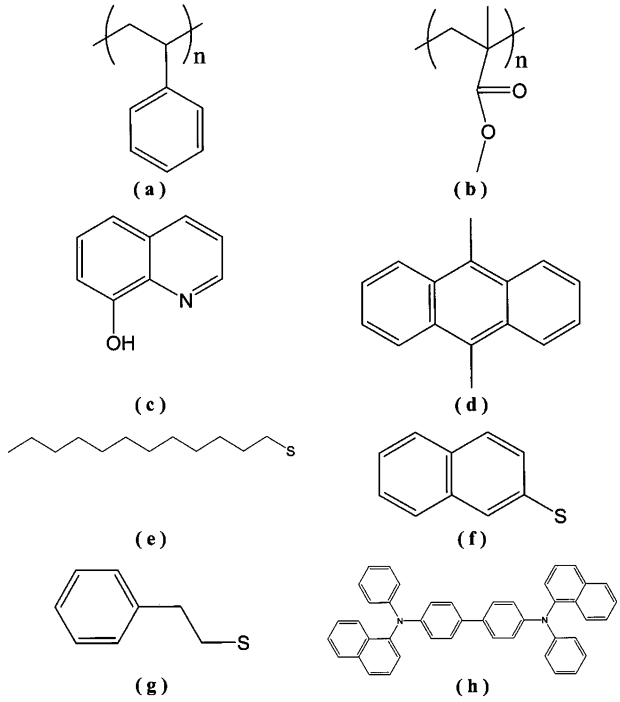

Fig. 2. Chemical structure of: (a) polystyrene (PS); (b) poly(methyl methacrylate) (PMMA); (c) 8-hydroxyquinoline (8HQ); (d) 9,10-dimethylanthracence (DMA); (e) 1-dodecanethiol (DT); (f) 2-naphthalenethiol (2NT); (g) 2-benzeneethanethiol; and (h) N,N′-bis(naphthalene-1-yl)-N,N′-bis(phenyl)benzidine (NPB).

II. Nonvolatile Polymer Memory Devices

Fig. 1 shows the device structure of our nonvolatile polymer memory device. This device has a simple architecture: a polymer film sandwiched between two metal electrodes. The polymer film consists of small conjugated organic compound and metal nanoparticle capped with saturated alkanethiol. The chemical structure of some materials presented in this paper is shown in Fig. 2. The metal nanoparticles were prepared by the two-phase arrested growth method [14]. The gold nanoparticles capped with DT had a narrow size distribution (1.6–4.4 nm in diameter) and an average particle size of 2.8 nm (Fig. 3).

The device using PS, gold nanoparticles capped with DT (Au-DT NP), and 8HQ was fabricated through the following process. The device using other materials was fabricated through a similar process. At first, the bottom aluminum (Al) electrode was thermally evaporated on a glass substrate in a very clean chamber with a vacuum of 10^{-5} torr. Then, the active layer between the two Al electrodes was fabricated

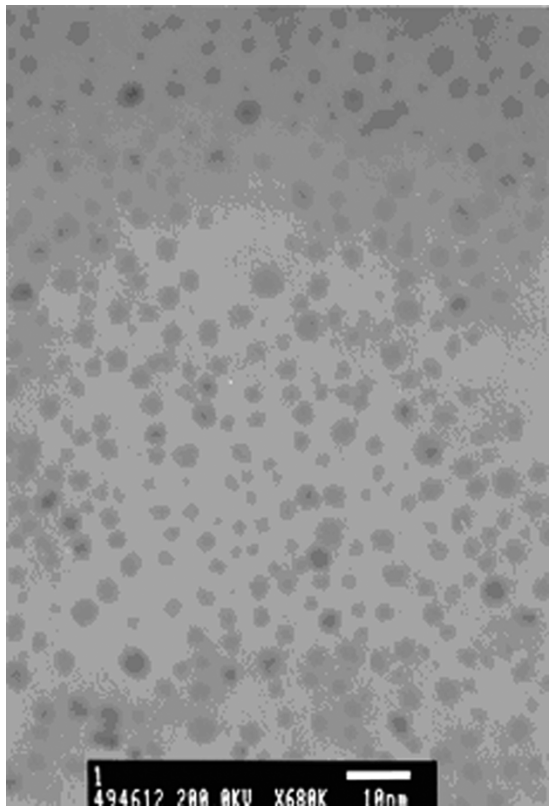

Fig. 3. Transmission electron microscope (TEM) image of Au-DT NPs.

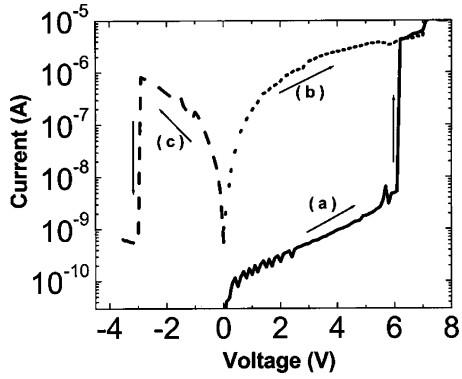

Fig. 4. I–V curves of the device, Al/Au-DT NP+DMA+PS/Al. (a), (b), and (c) represent the first, second, and third bias scans, respectively. The arrows indicate the voltage-scanning directions.

by spin coating a 1, 2-dichlorobenzenic solution of 0.4% by weight Au-DT NP, 0.4% by weight 8HQ, and 1.2% by weight PS. This organic film had a thickness of about 50 nm. Finally, the device was completed by thermal evaporation of the top Al electrode. The top and bottom Al electrodes had a linewidth of 0.2 mm and were aligned perpendicular to each other, so that the device had an area of 0.2×0.2 mm^2. This device is represented as Al/Au-DT NP+8HQ+PS/Al in this paper. When 8HQ is replaced by DMA, the device is denoted as Al/Au-DT NP+DMA+PS/Al.

Fig. 4 shows the I–V curves of Al/Au-DT NP+DMA+PS/Al in air, tested with an HP 4155B semiconductor parameter analyzer. The pristine device exhibited very low current, approximately 10^{-10} A at 1 V.

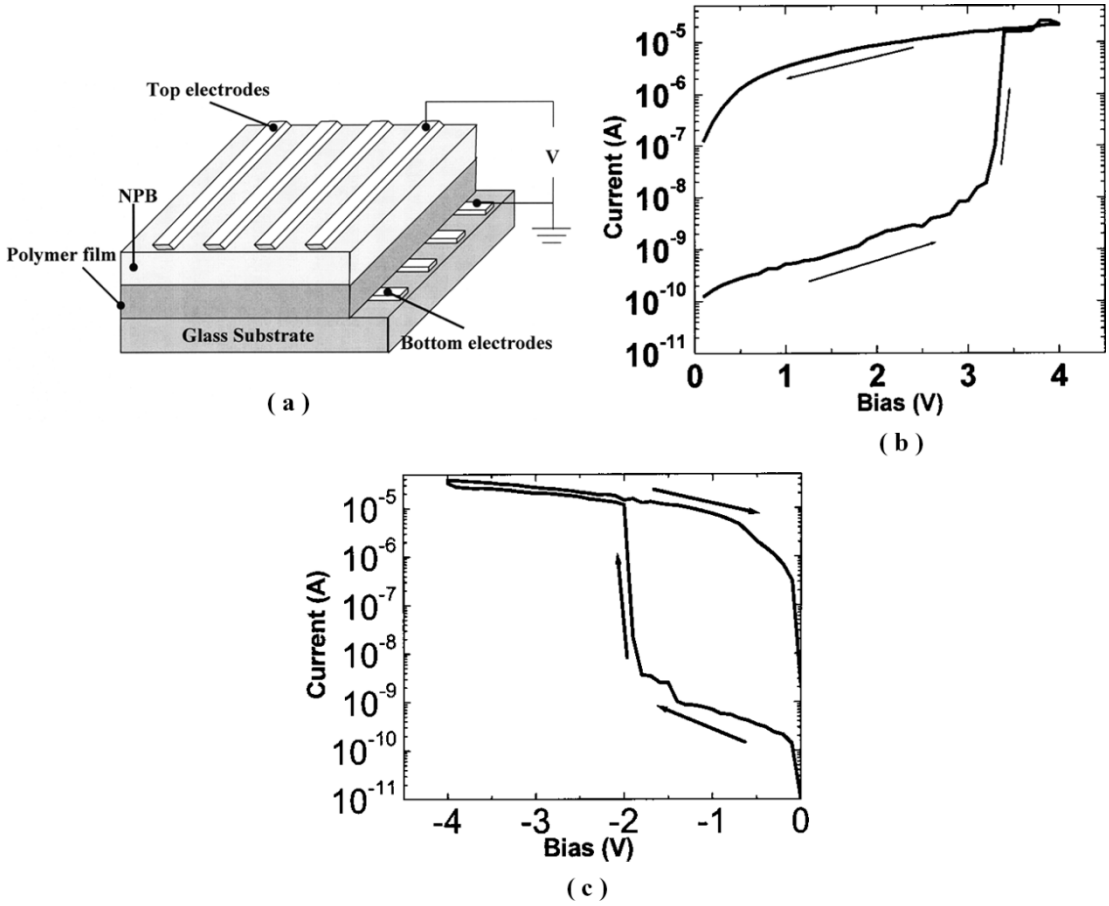

Fig. 5. (a) Device structure of Al (top)/NPB/Au-DT NP+8HQ+PS/Al (bottom)/glass. The bottom electrode is grounded. (b) I–V curves when the top electrode was positively biased. (c) I–V curves when the top electrode was negatively biased. The arrows in (b) and (c) denote the voltage-scanning directions.

An electrical transition took place at 6.1 V with an abrupt current increase from 10^{-9} to 10^{-6} A [curve (a)]. The device exhibited good stability in this high-conductivity state during the subsequent voltage scan [curve (b)]. The high-conductivity state was able to return to the low-conductivity state by applying a negative bias as indicated in curve (c) where the current suddenly dropped to 10^{-9} A at -2.9 V.

When the device was tested in a nitrogen atmosphere or in vacuum, it exhibited similar electrical behavior. The transition voltages and the current for the device in the high-conductivity state are almost the same as those tested in air, while the current for the device in the low-conductivity state is lower by one to two orders of magnitude than that tested in air. Hence, the conductivity difference for the device in the two conductivity states in vacuum could be more than four orders of magnitude.

Other materials were also used to fabricate the device to study the effect of materials on the device performance. When DMA was replaced with 8HQ, the device Al/Au-DT NP+8HQ+PS/Al exhibited similar behavior, but the transition voltages were lower. The threshold voltage from low- to high-conductivity state was at about 2.8 V, while the threshold voltage from high- to low-conductivity state appeared at about -1.8 V. When PS was replaced by PMMA, similar repeatable switching behavior between the two conductivity states was observed. Moreover, when the polymer film consisted of only PMMA and Au-DT NP without 8HQ or any other conjugated organic compound, no remarkable electrical transition was observed.

The Al electrode might oxidize in air. To investigate whether this oxidized Al layer contributed to the electrical transition and the effect of interface between the polymer layer and the electrode on the device performance, devices using other conductive materials, such as gold, copper, and indium–tin–oxide (ITO), as one or both electrodes were fabricated as well. These devices exhibited quite similar electrical behavior. A very thin aluminum oxide layer on the electrode does not affect the electrical transition.

On the other hand, it was observed that the insertion of an additional organic layer between the polymer film and the Al electrode changed the electrical behavior of the device. When the device had a structure of the polymer film sandwiched between the two Al electrodes, the switching behavior was symmetrical in the two polarities; that is, the transition voltage from low- to high-conductivity state took place at almost the same absolute voltage value regardless whether the top electrode was positively or negatively biased. However, asymmetrical switching behaviors were observed when an additional layer of NPB (thickness was 30 nm) was thermally deposited on the film consisting of Au-DT NP, 8HQ, and PS [device structure shown in Fig. 5(a)]. This de-

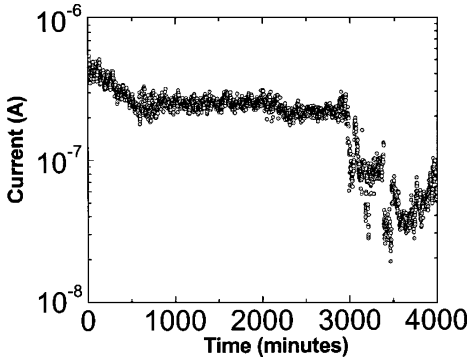

Fig. 6. Stress test of Al/Au-DT NP+8HQ+PS/Al in the high-conductivity state at 1 V in nitrogen.

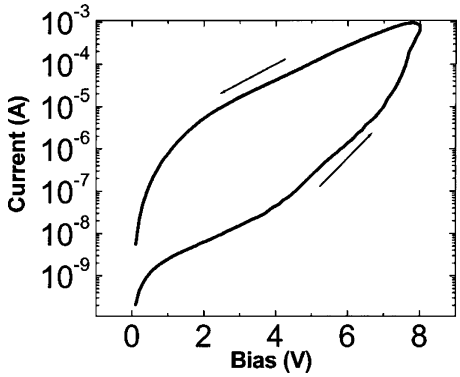

Fig. 7. I–V curves of the device Al/Au-2NT NP+PS/Al. The arrows indicate the voltage-scanning directions [13].

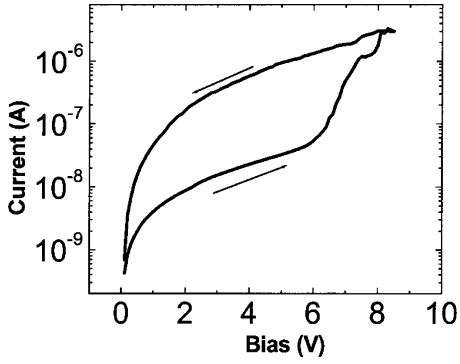

Fig. 8. I–V curves of the device Al/Au-BET NP+PS/Al. The arrows indicate the voltage-scanning directions.

vice is denoted by Al (top)/NPB/Au-DT NP+8HQ+PS/Al (bottom)/glass. The transition from low- to high-conductivity state appeared at about 3.3 V when the top electrode was positively biased [Fig. 5(b)], while it changed to about -1.9 V when electrical polarity was reversed [Fig. 5(c)].

The electrical switching between the high- and low-conductivity states of these bistable devices could be repeated numerous times. These two states could be programmed by applying a positive or negative voltage pulse. Hence, when the high- and low-conductivity states are defined as "1" and "0," respectively, this device can be used as a nonvolatile organic digital memory.

One important point for the application of a device as a nonvolatile electronic memory is the stability of the device in the two states. This device exhibited good stability in the two states. The device in the low-conductivity state always exhibited very low current under a constant voltage of 1 V. The stability in the high-conductivity state showed device dependence. We got a device which exhibited stability longer than 50 h (Fig. 6).

The device in the low-conductivity state can be switched to high-conductivity by a pulse of 5 V with a width of 25 ns. The device, which was in the low-conductivity state, exhibited current less than 10^{-9} A in the voltage range of 0–1 V. It exhibited a current four orders of magnitude higher after applying a pulse of 5 V with a width of 25 ns. At this time, our equipment (HP 214B Pulse Generator) was incapable of generating a pulse shorter than 25 ns. It is possible that this device is actually faster than that we are able to measure.

III. Write-Once-Read-Many Polymer Memory

The electrical behavior of the device was dependent on the chemical structure of the conjugated organic compounds and the metal nanoparticles in the polymer film. When the chemical structure of the capping molecule on the gold nanoparticle changed from a saturated thiol compound to an aromatic compound, the electrical behavior of the device significantly changed. A device using a PS film consisting of gold nanoparticles capped with 2NT (Au-2NT NP) was fabricated through a similar fabrication process as that of Al/Au-DT NP+8HQ+PS/Al. This device is represented by Al/ Au-2NT NP+PS/Al, and its *I–V* curve is shown in Fig. 7. At the first voltage scan, the current exhibited rapid increase starting from about 4 V, but this current increase was less abrupt than the device presented in Section II. After the voltage scan from 0 to 8 volt, the device transited to a high-conductivity state. The current at 2 V was different by about three orders in magnitude for the device in the two conductivity states. This device after transiting to the high-conductivity state could not return to the low-conductivity state by applying a negative voltage or a high voltage in either polarity.

The effect of the chemical structure of the gold nanoparticles was further investigated. A device using a PS film consisting of gold nanoparticle capped with 2-benzeneethanethiol (Au-BET NP) was fabricated as well. This device is represented by Al/ Au-BET NP+PS/Al, and its *I–V* curve is shown in Fig. 8. A rapid current increase started from about 6 V. This current increase as well was less abrupt than the device presented in Section II. The current at 2 V was different by less than two orders in magnitude for the device in the two conductivity states. The less current difference for Al/Au-BET NP+PS/Al than that of Al/Au-2NT NP+PS/Al may be due to less conjugated π-electrons on 2-benzeneethanethiol than those on 2NT, which are the capping molecules on the gold nanoparticles.

For these two devices using gold nanoparticles capped with aromatic thiols, the presence of other conjugated organic compound, such as 8HQ, did not affect the *I–V* curve. This is because conjugated structure has already been in the polymer film, and the aromatic group on the capped molecule

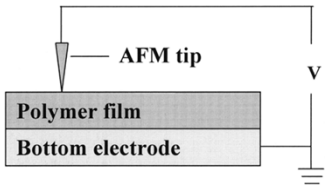

Fig. 9. Test configuration for the operation of the device using an AFM tip as the top electrode.

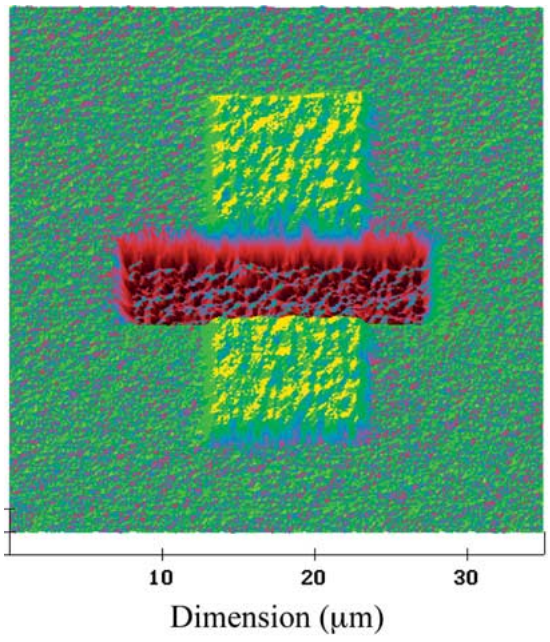

Fig. 10. Scanning surface potential AFM image of Au-DT NP+8HQ+PS film with Al as bottom electrode and silicon wafer as substrate. The vertical bar with yellow color was pretreated with a +10-V dc bias, while the horizontal bar with brown color was pretreated with a −10-V dc bias [12].

screens the interaction between the core of the gold nanoparticle and the conjugated compound.

These devices using gold nanoparticles capped with aromatic thiols can transit to a high-conductivity state and have good stability in the high-conductivity state. Therefore, these devices can be used as write-once-read-many-times memory devices.

IV. High-Density Memory Devices

These polymer memory devices have a simple device structure and could have very high density when high-density electrodes are fabricated. The device structure can be made even simple, and the density can be pushed to very high, when the operation of the device is combined with an atomic force microscope (AFM). A schematic configuration for this device is shown in Fig. 9. The device was fabricated by one step: the polymer film was spin coated on a conductive substrate. The conductive substrate was used as the bottom electrode, while an AFM tip was as the top electrode.

Fig. 10 shows a surface potential AFM picture of a Au-DT NP+8HQ+PS film on Al coated on silicon wafer. At first, an area of 20 μm × 10 μm of the film was scanned vertically in contact mode while positively applying 10-V dc bias through a 50-nm silicon nitride AFM tip coated with Au. Then, another area of 20 μm × 5 μm was scanned horizontally while applying a −10-V dc bias through the tip. Finally, the scanning surface potential image was taken with a tapping model. A dc bias of 4 V was applied on the film through the 50-nm AFM silicon nitride tip coated with Au. The two pretreated areas exhibited remarkably different potential in the surface potential AFM. These experiments demonstrated the feasibility of the device operated with an AFM.

V. Proposed Mechanism for Electrical Switching

A. Electric-Field-Induced Charge Transfer Between Gold Nanoparticle and 8HQ

The nanosecond-scale transition of these devices suggests that the switching process may be an electronic process rather than chemical rearrangement, conformational change, or isomerization. For example, conformational change for a ferroelectric polymer occurs on a 30-μs time scale [5]. Atomic movement or molecular isomerization that can result in electrical bistability is observed on molecular devices [15], [16]; however, the transition time is on the millisecond time scale or even longer. We study the switching mechanism by ac impedance spectroscopy and a study of the transport mechanisms and the energy levels of the materials.

Our experimental results suggest that the switching mechanism is not due to the formation of conductive filaments between the two metal electrodes, which was observed in a polymer film by others [17], [18]. It is unlikely that filament formation is the reason for the electronic transitions in our device, since the electrical behavior of our device is strongly dependent on the structure and the concentration of the gold nanoparticles. In addition, ac impedance studies, from 20 to 10^6 Hz (Fig. 11), indicate that the electronic transitions in our device are different from the dielectric breakdown found in polymer films. We observed dielectric breakdown in a device with a PS film sandwiched between two Al electrodes. After breakdown, the current increased by more than four orders of magnitude, and the capacitance was lowered by about one order of magnitude. In comparison, Al/Au-DT NP+8HQ+PS/Al exhibited an increase in current by more than four orders of magnitude. The capacitance increased in the low-frequency range while remaining the same in the high-frequency range after a pristine device was turned to the high-conductivity state. This suggests that space charges may generate in the film after the as-prepared device is electrically turned to a high-conductivity state. PS may act as an inert matrix for Au-DT nanoparticles and 8HQ and may not play a role in the electronic transition. So we exclude from our model changes in electrical behavior based on slow-speed switching mechanisms and filament formation.

The conduction mechanism for Al/Au-DT NP+8HQ+PS/Al in the low-conductivity state may be due to a quite small amount of impurity or hot electron injection. The current for the device in the high-conductivity state was almost temperature independent (Fig. 12), and the I–V curves can be fitted well by a combination of

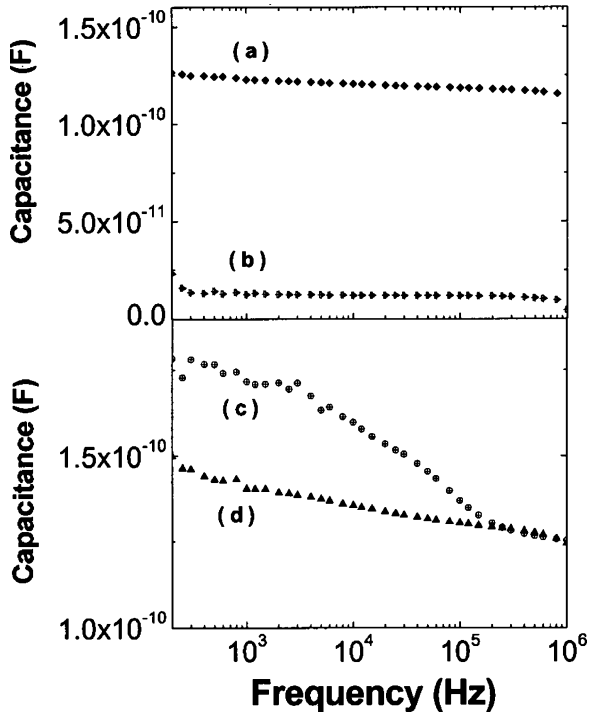

Fig. 11. Capacitance of: (a) pristine Al/PS/Al; (b) Al/PS/Al after breakdown; (c) Al/Au-DT NP+8HQ+PS/Al in high-conductivity state; and (d) pristine Al/Au-DT NP+8HQ+PS/Al.

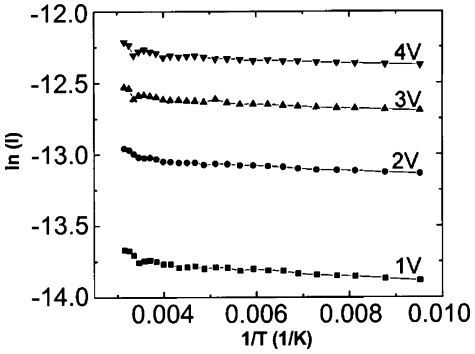

Fig. 12. Arrhenius plot of temperature dependence of current for Al/Au-DT NP+8HQ+PS/Al in the high-conductivity state at applied voltages of 1, 2, 3, and 4 V (Reference [12]).

direct tunneling (tunneling through a square barrier) and Fowler–Nordheim tunneling (tunneling through a triangular barrier) (Fig. 13) as given by the following expression [19]:

$$I = C_1 V e^{-\frac{2d\sqrt{2m*\Phi}}{\hbar}} + C_2 V^2 e^{-\frac{4d\Phi^{\frac{3}{2}}\sqrt{2m^*}}{3q\hbar V}}.$$

The first term on the right-hand side of the equation is the current contributed by direct tunneling, and the second term is the current contributed by Fowler–Nordheim tunneling. In this equation, d is the tunneling distance, m^* is the effective mass of the charge carrier, and Φ is the energy barrier height. At low voltage, $V < \Phi$, direct tunneling is the dominant conduction mechanism, and at high voltage, $V > \Phi$, Fowler–Nordheim tunneling becomes the dominant conduction mechanism.

The different conduction mechanisms in the two states suggest change in the electronic structure of the device after

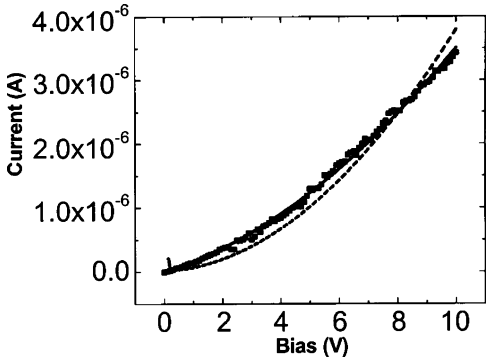

Fig. 13. I–V curve of the device Al/Au-DT+8HQ+PS/Al in the high-conductivity state [12]. The scattered points are the experimental results, the solid line is the data fit combining direct tunneling and Fowler–Nordheim tunneling, and the broken line is the data fit of Fowler–Nordheim tunneling.

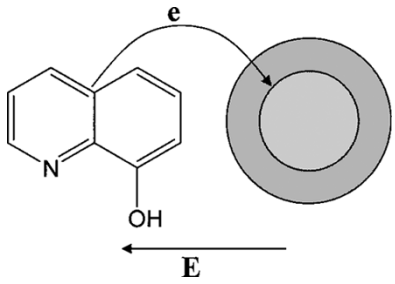

Fig. 14. Schematic electron transfer from 8HQ to the core of the gold nanoparticle. The yellow circle indicates the core of the gold nanoparticle, and the gray ring indicates the capped DT. The curved arrow denotes the electron transfer from 8HQ to the core of gold nanoparticle; **e** denotes the electron. The direction of the electric field (**E**) is represented by the linear arrow.

the electrical transition. It has already been demonstrated that 8HQ and gold nanoparticle can act as electron donor and acceptor, respectively [20]–[23]. Moreover, the different surface potentials of the Au-DT NP+8HQ+PS film after the treatment by different electric fields as shown in Fig. 10 suggest that the electric field can induce the polarization of the film. Hence, we propose a charge transfer between Au-DT NP and 8HQ under a high electric field for the electronic transition in Al/Au-DT NP+8HQ+PS/Al. Prior to the electronic transition, there is no interaction between the Au-DT nanoparticle and 8HQ. Concentration of charge carriers due to impurity in the film is quite low, so that the film has very low conductivity. However, when the electrical field increases to a certain value, electron on the highest occupied molecular orbital (HOMO) of 8HQ may gain enough energy to tunnel through the capped molecule, DT, into the gold nanoparticle (Fig. 14). Consequently, the HOMO of 8HQ becomes partially filled, and 8HQ and gold nanoparticle are charged positively and negatively, respectively. Therefore, carriers are generated and the device exhibits a high-conductivity state after the charge transfer. It is well-known that the conductivity of conjugated organic compounds will increase after their HOMO or lowest occupied molecular orbital (LUMO) becomes partially filled [7], [24], [25].

For the device in the high-conductivity state, the charge transport through the polymer film may take place through charge tunneling among the 8HQ molecules. The separation

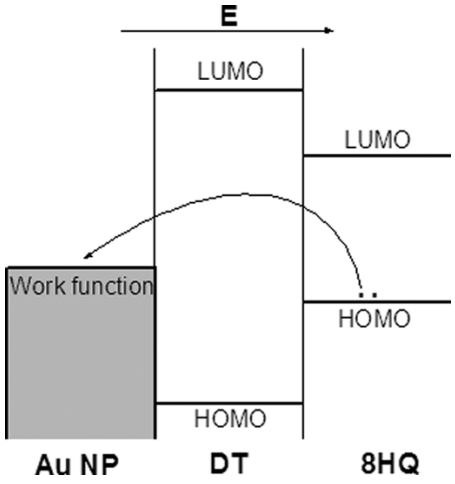

Fig. 15. Energy diagram of the core of gold nanoparticle, DT, and 8HQ. The two dots on the HOMO of 8HQ represent two electrons. The linear arrow indicates the direction of the electric field (**E**), and the curved arrow indicates the electron transfer from 8HQ to the core of gold nanoparticle.

among the 8HQ molecules in the polymer film will become larger than that in the 8HQ crystal. A simple estimation suggests that the separation among the 8HQ molecules in the Au-DT NP+8HQ+PS film is about 6–10 Å. For such a separation, it is reasonable that the tunneling process becomes the dominant charge transport mechanism among the 8HQ molecules.

This simple model can interpret the stability of the device in the high-conductivity state as well as the erasing process by applying a negative bias. Stability of the negative charge on gold nanoparticle is due to the insulator coating, DT, on the gold nanoparticles, which prevents recombination of the charge after removal of the external electric field. Since the charge transfer is induced by an external electrical field, the film is polarized after the charge transfer. Only a reverse electric field can assist the tunneling of the electron from the gold nanoparticle back to the HOMO of $8HQ^{+}$, resulting in a return to the low-conductivity state.

This electric-field-induced charge transfer model explains quite well the electronic transition observed in the device Al/Au-DT NP+8HQ+PS/Al and is supported by the evidence noted above as well as the following additional evidence: fast switching speed, lack of dielectric breakdown, temperature-insensitive conductivity, and device performance dependence on the gold nanoparticle concentration and size. Charge tunneling through the insulator coating on the gold nanoparticle is possible, as required by our model. For example, it has been observed frequently, by electrochemical measurements, that gold nanoparticles coated with an insulating alkanethiol layer can be reduced or oxidized [26], [27]. Fig. 15 shows the energy levels of gold nanoparticle and 8HQ and the electron transfer from the HOMO level of 8HQ to the core of the gold nanoparticle. The HOMO and LUMO levels of 8HQ, calculated using the DFT B3LYP method with the $6-31+G(d,p)$ basis set, are 1.9 and 6.1 eV, respectively. The quantized energy δ for a gold nanoparticle with a diameter of 2.8 nm is about 0.014 eV calculated in terms of this equation [28]:

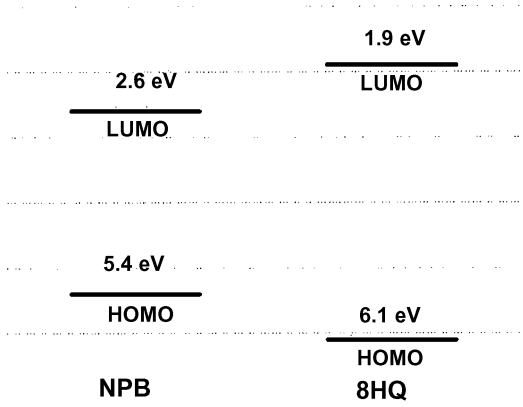

Fig. 16. Energy diagram of 8HQ and NPB.

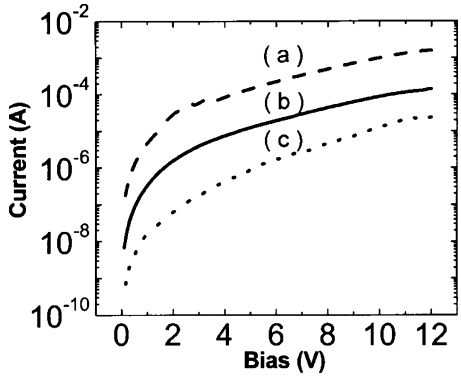

Fig. 17. I–V curve of Al/Au-2NT NP+PS/Al with different Au-2NT NP concentrations in the high-conductivity state. (a) 1%. (b) 0.4%. (c) 0.1%.

$$\delta = \frac{4E_F}{3N}$$

where E_F is the Fermi energy of bulk Au and N denotes the number of Au atoms in one gold nanoparticle. This quantized energy is even much smaller than the thermal energy at room temperature, so that its effect can be neglected. On the other hand, the Coulomb energy (E_c) to charge a gold nanoparticle, with a diameter of 2.8 nm and capped with DT, is about 0.1 eV, calculated by the following equation [29]:

$$E_c = \frac{e^2}{2C}$$
$$\text{and } C = 4\pi\varepsilon_0\varepsilon_r\frac{r}{d}(r+d)$$

where C is the capacitance of the gold nanoparticle, ε_0 the permittivity of free space, ε_r the permittivity of the capped molecule on the gold nanoparticle, r the radius of the gold nanoparticle core, and d the length of the capped molecule. This charging energy is the energy to be overcome for the charge transfer to take place. It is possible for the electron to gain such energy under a high electric field. These considerations on the energies suggest that a charge transfer from 8HQ to gold nanoparticle is possible under the application of a high electric field.

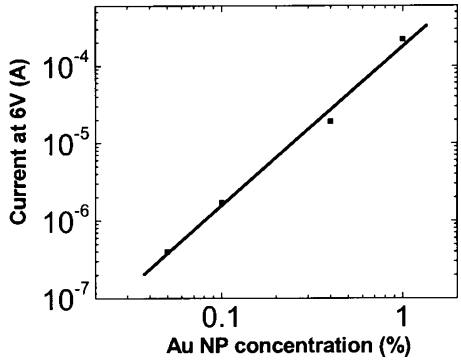

Fig. 18. Dependence of current at 6 V on the Au-2NT NP concentration for device Al/Au-2NT NP+PS/Al in the high-conductivity state. The scatters are the experimental data, and the line is a best fitting on the data.

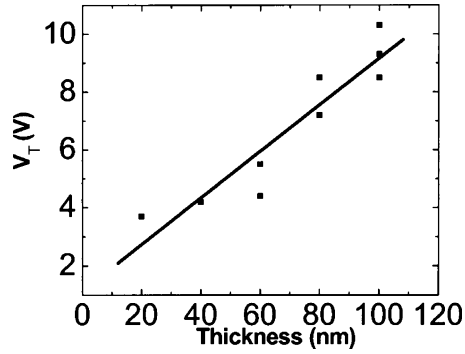

Fig. 19. Dependence of transition voltage on the film thickness for the device Al/Au-2NT NP+PS/Al. The scatters are the experimental data, and the line is a best fitting on the data.

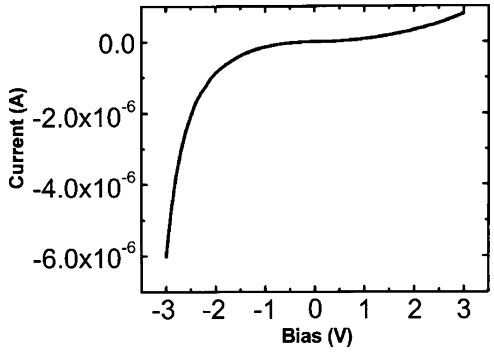

Fig. 20. Asymmetric *I–V* curve of Al/Au-2NT NP+PS/Al in the high-conductivity state [13].

The asymmetrical switching behavior for the device Al (top)/NPB/Au-DT NP+8HQ+PS/Al (bottom)/glass can be interpreted based on the energy levels of NPB and 8HQ and the proposed charge-transfer mechanism. NPB has a HOMO level (5.4 eV) higher than the HOMO level (6.1 eV) of 8HQ (Fig. 16), so that a barrier exists at the interface between NPB and 8HQ for a hole transport from NPB to 8HQ, while such a barrier disappears when the hole transports in the reverse direction. This is consistent with the different threshold voltages for the transition from low- to high-conductivity states in the two biased directions.

B. Electric-Field-Induced Charge Transfer Between the Core of Gold Nanoparticle and Capping 2NT

We propose that the electrical transition for the device Al/Au-2NT NP+PS/Al is due to an electric-field-induced charge transfer between core of the gold nanoparticle and the capping conjugated molecule. This assumption is supported by the following experimental results. Fig. 17 is the *I–V* curve of Al/Au-2NT NP+PS/Al fabricated with different Au-2NT NP concentration in the solution in the high-conductivity state. The current increases with the increase of the Au-2NT NP concentration. Fig. 18 plots the current at 6 V versus the Au-2NT NP concentration. A best fitting of these data indicates that the current is proportional to the square of the concentration. These results suggest that the Au-2NT NP is the media for the charge transport through the film due to the conjugated naphthalene structure. This is different from the film of Au-DT NP+8HQ+PMMA, of which there is only 8HQ with conjugated quinoline structure and 8HQ is the media for the charge transfer through the film.

The effect of film thickness on the transition voltage was investigated as well (Fig. 19). The transition voltage for Al/Au-2NT NP+PS/Al was not as easy to distinguish as that for Al/Au-DT NP+DMA+PS/Al. The transition voltage was defined as the voltage at which the current starts a rapid increase in the $\log I$ versus V graph. The transition voltage for some devices exhibited scattered values, and all these voltages were plotted. The transition voltage increases linearly with the increase of the film thickness. This linear relation indicates that the electrical transition is a result of an electric-field effect.

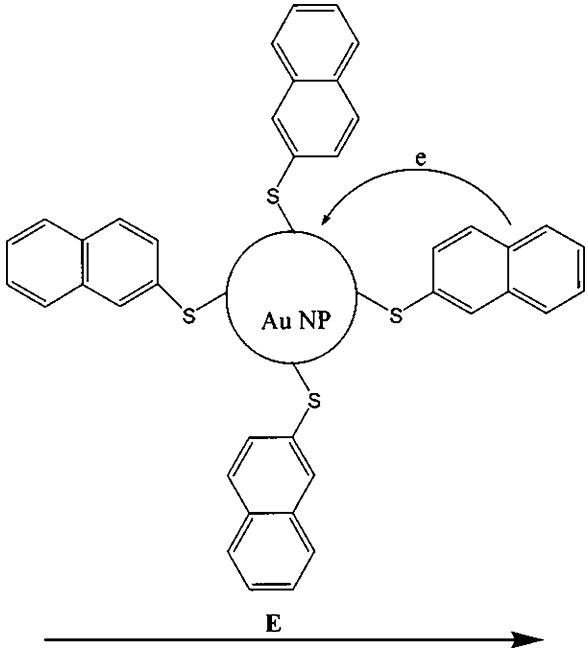

Fig. 21. Schematic electron transfer from capping molecule 2NT to the core of the gold nanoparticle. Only four 2NT molecules are plotted to represent all capping 2NT molecules on the gold nanoparticle. The curved arrow indicates the electron (**e**) transfer. The linear arrow denotes the direction of the electric field (**E**).

The electric-field induced charge transfer in the polymer film is further evidenced by the asymmetric *I–V* curve for the device in the high-conductivity state. The *I–V* curve was

symmetric in the two polarity directions in the voltage range below 3 V before the transition, while it became asymmetric after the transition. If the polarity direction that resulted in the transition was defined as positive, the current along the negative direction was higher than along the positive direction. (Fig. 20) The current at -3 V reached almost ten times as that at 3 V. This asymmetric I–V curve after the transition suggests that the electric field may induce a polarization of the Au-2NT NP in the polymer film.

This polarization is interpreted as the result of a high electric-field-induced charge transfer between the gold nanoparticle and the capping 2NT: the capping 2NT donates an electron to the core of the gold nanoparticle (Fig. 21). After the charge transfer, the Au-2NT NP polarizes along the applied electric field. Hence, the device will have higher current when the external electric field is applied along this polarization direction than that when the external electric field is applied against this polarization.

This model can explain the two conductivity states well. Before the transition, the current is controlled by the charge injection from the electrode into the polymer film due to a big energy barrier between the Al electrode and Au-2NT NPs. After the charge transfer between the Au nanopaticle and 2NT induced by a high electric field, 2NT is positively or negatively charged so that the film exhibits a high current.

VI. Summary

Both nonvolatile and write-once-read-many-times electronic memory devices in a polymer version were demonstrated. These devices by exploiting an electric-field-induced charge transfer between the metal nanoparticle and conjugated organic structure have a very strong potential application as an ultrahigh density and ultrafast electronic memory. This device has remarkable advantages. The materials used in this device are readily available and easily controlled, the device can be fabricated through a simple solution processing approach, the response time is very short, and the operating voltages are low. The device has a high flexibility so that it is compatible with other organic devices. In addition, a device with multiple active layers could be readily constructed so that the density could be further increased. This last advantage is significant compared to traditional inorganic semiconductor memory, which is restricted to two dimensions.

Acknowledgment

The authors would like to thank D. Sievers for calculating the HOMO–LUMO levels of 8HQ and 2NT.

References

[1] J. H. Burroughes, D. D. C. Bradley, A. R. Brown, R. N. Marks, K. Mackay, R. H. Friend, P. L. Burns, and A. B. Holmes, "Light-emitting diodes based on conjugated polymers," *Nature*, vol. 347, pp. 539–541, 1990.

[2] C. W. Tang and S. A. Vanslyke, "Organic electroluminescent diodes," *Appl. Phys. Lett.*, vol. 51, pp. 913–915, 1987.

[3] N. S. Sariciftci, L. Smilowitz, A. J. Heeger, and F. Wudl, "Photoinduced electron-transfer from a conducting polymer to buckminsterfullerene," *Sciene*, vol. 258, pp. 1474–1476, 1992.

[4] C. D. Dimitrakopoulos and D. J. Mascaro, "Organic thin-film transistors: a review of recent advances," *IBM J. Res. Dev.*, vol. 45, pp. 11–27, 2001.

[5] T. Furukawa, "Structure and functional properties of ferroelectric polymer," *Adv. Colloid Interface Sci.*, vol. 71–72, pp. 183–208, 1997.

[6] R. S. Potember, T. O. Poehler, and R. C. Benson, "Electrical switching and memory phenomena in Cu-TCNQ thin films," *Appl. Phys. Lett.*, vol. 34, pp. 405–407, 1982.

[7] T. Oyamada, H. Tanaka, K. Matsushige, H. Sasabe, and C. Adachi, "Switching effect in Cu: TCNQ charge transfer-complex thin films by vacuum codeposition," *Appl. Phys. Lett.*, vol. 83, pp. 1252–1254, 2003.

[8] L. P. Ma, J. Liu, and Y. Yang, "Organic electrical bistable devices and rewritable memory cells," *Appl. Phys. Lett.*, vol. 80, pp. 2997–2999, 2002.

[9] L. P. Ma, S. Pyo, J. Ouyang, Q. F. Xu, and Y. Yang, "Nonvolatile electrical bistability of organic/metal-nanocluster/organic system," *Appl. Phys. Lett.*, vol. 82, pp. 1419–1421, 2003.

[10] L. D. Bozano, B. W. Kean, V. R. Deline, J. R. Salem, and J. C. Scott, "Mechanism for bistability in organic memory elements," *Appl. Phys. Lett.*, vol. 84, pp. 607–609, 2004.

[11] S. Möller, C. Perlov, W. Jackson, C. Taussig, and S. F. Forrest, "A polymer/semiconductor write-once read-many-times memory," *Nature*, vol. 426, pp. 166–169, 2003.

[12] J. Ouyang, C.-W. Chu, C. Szmanda, L. Ma, and Y. Yang, "Programmable polymer thin film and nonvolatile memory device," *Nature Mater.*, vol. 3, pp. 918–922, 2004.

[13] J. Ouyang, C.-W. Chu, D. Sievers, and Y. Yang, "Electric-field-induced charge transfer between gold nanoparticle and capping 2-naphthalenethiol and organic memory cells," *Appl. Phys. Lett.*, vol. 86, p. 123 507, 2005.

[14] M. J. Hostetler, J. E. Wingate, C. J. Zhong, J. E. Harris, R. W. Vachet, M. R. Clark, J. D. Londono, S. J. Green, J. J. Stokes, G. D. Wignall, G. L. Glish, M. D. Porter, N. D. Evans, and R. W. Murray, "Alkanethiolate gold cluster molecules with core diameters from 1.5 to 5.2 nm: core and monolayer properties as a function of core size," *Langmuir*, vol. 14, pp. 17–30, 1998.

[15] Y. Chen, D. A. A. Ohlberg, X. M. Li, D. R. Stewart, R. S. Williams, J. O. Jeppesen, K. A. Nielsen, J. F. Stoddart, D. L. Olynick, and E. Anderson, "Nanoscale molecular-switch devices fabricated by imprint lithography," *Appl. Phys. Lett.*, vol. 82, pp. 1610–1612, 2003.

[16] T. Tsujioka and H. Kondo, "Organic bistable molecular memory using photochromic diarylethene," *Appl. Phys. Lett.*, vol. 83, pp. 937–939, 2003.

[17] H. K. Henish and W. R. Smith, "Switching in organic polymer films," *Appl. Phys. Lett.*, vol. 24, pp. 589–591, 1974.

[18] Y. Segui, B. Ai, and H. Carchano, "Switching in polystyrene films: transition from on to off state," *J. Appl. Phys.*, vol. 47, pp. 140–143, 1976.

[19] W. Wang, T. Lee, and M. A. Reed, "Mechanism of electron conduction in self-assembled alkanethiol monolayer devices," *Phys. Rev. B*, vol. 68, p. 035 416, 2003.

[20] C. K. Prout and A. G. Wheeler, "Molecular complexes. Part VII. The crystal and molecular structure of the 8-hydroxyquinoline chloranil complex," *J. Chem. Soc. A*, pp. 469–475, 1967.

[21] E. Castellano and C. K. Prout, "Molecular complexes. Part X. The crystal and molecule structure of the 1:1 complex of 8-hydroxyquinoline and 1,3,5-trinitrobenzene," *J. Chem. Soc. A*, pp. 550–553, 1971.

[22] D. M. Adams, L. Brus, C. E. D. Chidsey, S. Creager, C. Creutz, C. R. Kagan, P. V. Kamat, M. Lieberman, S. Lindsay, R. A. Marcus, R. M. Metzger, M. E. Michel-Beyerle, J. R. Miller, M. D. Newton, D. R. Rolison, O. Sankey, K. S. Schanze, J. Yardley, and X. Y. Zhu, "Charge transfer on the nanoscale: current status," *J. Phys. Chem. B*, vol. 107, pp. 6668–6697, 2003.

[23] B. I. Ipe, K. G. Thomas, S. Barazzouk, S. Hotchandani, and P. V. Kamat, "Photoinduced charge separation in a fluorophore-gold nanoassembly," *J. Phys. Chem. B*, vol. 106, pp. 18–21, 2002.

[24] T. Oyamada, H. Tanaka, K. Matsushige, H. Sasabe, and C. Adachi, "Switching effect in Cu: TCNQ charge transfer-complex thin films by vacuum codeposition," *Appl. Phys. Lett.*, vol. 83, pp. 1252–1254, 2003.

[25] X.-L. Mo, G.-R. Chen, Q.-J. Cai, Z.-Y. Fan, H.-H. Xu, Y. Yao, J. Yang, H.-H. Gu, and Z.-Y. Hua, "Preparation and electricalyoptical bistable property of potassium tetracyanoquinodimethane thin films," *Thin Solid Films*, vol. 436, pp. 259–263, 2003.

[26] S. Chen, R. S. Ingram, M. J. Hostetler, J. J. Pietron, R. W. Murray, T. G. Schaaff, J. T. Khoury, M. M. Alvarez, and R. L. Whetten, "Gold nanoelectrodes of varied size: transition to molecule-like charging," *Science*, vol. 280, pp. 2098–2101, 1998.
[27] J. F. Hicks, A. C. Templeton, S. W. Chen, K. M. Sheran, R. Jasti, R. W. Murray, J. Debord, T. G. Schaaf, and R. L. Whetten, "The monolayer thickness dependence of quantized double-layer capacitances of monolayer-protected gold clusters," *Anal. Chem.*, vol. 71, pp. 3703–3711, 1999.
[28] R. Kubo, "Electronic properties of metallic fine particles. I," *J. Phys. Soc. Jpn.*, vol. 17, pp. 975–986, 1962.
[29] S. Chen, R. W. Murray, and S. W. Feldberg, "Quantized capacitance charging of monolayer-protected Au clusters," *J. Phys. Chem. B*, vol. 102, pp. 9898–9907, 1998.

Jianyong Ouyang received the B.S. degree in chemistry from the Tsinghua University, Beijing, China, in 1993, the M.S. degree in chemistry from the Institute of Chemistry, Chinese Academy of Sciences, in 1996, and the Ph.D. degree in solid state chemistry from the Graduate University for Advanced Studies (Institute for Molecular Science), Japan, in 1999.

He was a Research Associate at the Japanese Advanced Institute of Science and Technology from April 2000 to January 2001. He has been a Postdoctoral Researcher at Prof. Y. Yang's laboratory at the University of California, Los Angeles, since 2001. He had extensive research experience in the interdisciplinary fields of chemistry, physics, and materials science. Currently, his research is focusing on the development and characterization of organic electronic materials, nanometer materials, and novel electronic devices using organic materials and nanometer materials.

Chih-Wei Chu received the M.S. degree in civil and environmental engineering from the University of California, Los Angeles, in 1998. He is currently working toward the Ph.D. degree in Dr. Y. Yang group at the University of California, Los Angeles.

His primary research interests include organic thin-film transistors, organic solar cells, and organic bistable devices, with special emphasis on understanding mechanism and material development for organic bistable devices applied to data storage technology.

Ricky Jia-Hung Tseng received the B.S. and M.S. degrees in materials science and engineering from National Tsing Hua University, Taiwan, in 1998 and 2000 respectively. He is currently working toward the Ph.D. degree in materials science and engineering at the University of California, Los Angeles (UCLA).

He joined Prof. Y. Yang's group developing a nanocomposite bistable devices for memory applications. He interns with the Focus Center on Functional Engineered Nano Architectonics (FENA), the UCLA Nanoelectronics Research Laboratory, and Department of Chemistry and Biochemistry, UCLA. His recent research focuses on polymeric nanofiber memory devices and X-ray photoelectron characterization of polymer charge transfer systems, and biomaterials.

Ankita Prakash received the B.Tech. degree in material science and engineering from the Indian Institute of Technology (IIT), Kanpur, India, in 2002. She is currently working toward the M.S. from the University of California, Los Angeles (UCLA), and is doing research on polymer memory in Prof. Y. Yang's laboratory.

She worked for one year on a research project on Semiconducting Nanoparticles at the Indian Institute of Sciences (IISc), Bangalore, India. Her research interests include metallic and semiconducting nanoparticles, conducting polymers, and polymer electronic devices.

Yang Yang received the Ph.D. degree in physics and applied physics from the University of Massachusetts, Lowell, in 1992, under the supervision of Prof. J. Kumar and the late Prof. S. K. Tripathy.

He is a Professor in the Department of Materials Science and Engineering at the University of California, Los Angeles. Currently, his group has five postdocs/visiting scholars and 15 students. He also serves on the boards of several companies and government committees. He is a cofounder of ORFID Corp., a start-up company located in Los Angeles focusing on organic transistor for displays and organic RFID. He has published more than 100 refereed papers, given more than 50 invited presentations on his research work, and has filed or been granted 22 U.S. patents. His research focuses on conjugated organics and polymer materials and devices, such as LEDs, memory devices, transistors, and solar cells.

Prof. Yang has received the Outstanding Overseas Young Chinese Scientist Award from the Natural Science Foundation of China (2004), the National Science Foundation Career Award (1998), and the 3M Young Investigator Funds (1998).